# Role of $sp^2$ phase in field emission from nanostructured carbons

A. Ilie,[a] A. C. Ferrari, T. Yagi, S. E. Rodil, and J. Robertson
*Department of Engineering, Cambridge University, Cambridge CB2 1PZ, United Kingdom*

E. Barborini and P. Milani
*INFM-Dipartimento di Fisica, Universita di Milano, via Celoria 16, 20133 Milano, Italy*

(Received 30 October 2000; accepted for publication 30 April 2001)

It is shown that $sp^2$ phase organization plays an important role in the field emission from nanostructured carbons. Emission is found to depend on the cluster size, anisotropy, and mesoscale bonding of the $sp^2$ phase, and the electronic disorder. It is found by Raman spectroscopy that increasing the size of $sp^2$ clusters in the 1–10 nm range improves emission. Anisotropy in the $sp^2$ phase orientation can help or inhibit the emission. $sp^2$ clusters embedded in the $sp^3$ matrix or electronic disorder induced by localized defects oriented in the field direction can provide a local field enhancement to facilitate the emission. © *2001 American Institute of Physics.*
[DOI: 10.1063/1.1381001]

## I. INTRODUCTION

Carbon films with internal nanostructure have proved to be better electron field emitters, with a much higher site density and lower threshold field, than homogeneous amorphous carbon films. Some of these nanostructured films have mixed diamond/graphite phases, e.g., nanocrystalline diamond[1–3] or nanocrystalline–diamond/pyrocarbon composites.[4] In these cases, the graphitic phase is some 10%, but concentrated at the boundaries of the diamond crystallites, or in a thin shell ($\sim$1 nm) around the diamond crystallites.[4] Other good emitters have, in contrast, mainly $sp^2$ bonding. These can be synthesized using various deposition methods. High temperature plasma or hot filament chemical vapor deposition leads to nanocrystalline (corn-flake like) graphitic films.[5,6] The cathodic arc is a versatile deposition method since it allows various good emitters to be obtained at room temperature, from nanostructures embedded in an amorphous matrix[7,8] to the coralline material of Coll *et al.*[9] Preliminary studies have shown that good emission properties can also be obtained from cluster-assembled carbon (ca-C) deposited using supersonic beams.[10]

Studies performed on amorphous carbon systems have shown that, in these cases, the electron affinities involved are high,[11–13] leading to emission barriers of about 4–5 eV.[14] Emission also appears to originate from near the Fermi level in the case of nanocrystalline diamond.[3] There are also recent reports of emission from above the Fermi level, in the case of clean nanotubes[15] or nanodiamond–pyrocarbon.[4] In these cases, localized states induced by the low dimensionality of the tubes, and two-dimensional quantum well effects were invoked. However, we consider these latter cases less relevant for the wider class of nanostructured carbons, and expect emission to originate from sites with large emission barriers. This requires, in compensation, high local fields, which can be achieved through a high aspect ratio geometry, or by internal inhomogeneities.[16–18] As in most cases film roughness is not sufficient to generate a high enough field, the source of field enhancement has to be internal.

Here we focus on systems with bulk nanostructure, induced either directly during deposition or by postdeposition treatment. First, amorphous carbons (*a*-C) can be nanostructured by postdeposition annealing. These are good model systems as the $sp^2$ phase can be made to evolve inside the $sp^3$ matrix in a controllable way by increasing the annealing temperature. We show that in this way the $sp^2$ clusters increase in size and eventually adopt a preferential two-dimensional (2D) orientation as in graphite. Second, as-deposited nanostructured films were obtained by quenching a carbon ion plasma in a background inert gas, as described in Ref. 8, or by supersonic cluster beam expansion.[19,20] In contrast to the postdeposition nanostructured *a*-C's, these films are more complex, with a mesoscale structure and a tridimensional (3D) topology. Planar rings and cage-like clusters can be found embedded in an amorphous matrix.[19,21]

A comparison of all these films allows us to emphasize the effect of different $sp^2$ phase parameters, such as cluster size, orientation, and electronic disorder on field emission. We show that these are important factors controlling the emission. The evolution of the $sp^2$ phase was monitored using a combination of Raman spectroscopy, electron energy loss spectroscopy (EELS), resistivity, and work function measurements. An in-plane correlation length (size) of the $sp^2$ clusters was obtained from Raman. Information about the orientation of the $sp^2$ clusters in the amorphous $sp^3$ matrix was obtained here from resistivity, so that for annealed *a*-C's we could correlate anisotropy in conduction with an anisotropic development of the $sp^2$ phase.

We find that emission improves by increasing the Raman correlation length of $sp^2$ clusters in the 1–10 nm range. Orientation of the $sp^2$ phase matters, so that graphitic planes oriented perpendicular to the emission direction are unfavourable to emission. In contrast, films with graphitic planes oriented mainly parallel to the emission direction or with a 3D nanostructure can be better emitters. Reasons for

[a]Author to whom correspondence should be addressed; electronic mail: ai205@eng.cam.ac.uk

 

this behavior are discussed and related to the properties of the $sp^2$ phase.

## II. EXPERIMENTAL METHODS

*a*-C's can be nanostructured by giving energy to the system; either by thermal activation as in deposition at high temperatures or postdeposition annealing, or by atom displacement by knock-on in the case of high energy irradiation. Two microscopic processes take then place: (i) $sp^2$ phase clustering, and (ii) $sp^3$ to $sp^2$ conversion.

Here we consider postdeposition annealing of ta-C:N, ta-C:H, and *a*-C:H. All are diamond-like carbons, with an initial $sp^3$ content of 85%, 68%, and 65%, respectively. We chose these *a*-C's since hydrogen and nitrogen evolution induced by annealing allows them to undergo transformations in a greater degree than ta-C annealed at the same temperatures. Though *a*-C:H and ta-C:H have the same $sp^2$ content, ta-C:H has a better thermal stability. The effect of postdeposition annealing on field emission from ta-C has been shown elsewhere.[18] Annealing was carried out for 20 min in a vacuum of about $10^{-7}$ mbar, up to 700 °C for *a*-C:H, and up to 1000 °C for ta-C:H and ta-C:N. Film thickness was found to decrease slightly, by about 10%–20%, at the highest temperatures only.

As-deposited nanoclustered films were obtained through two deposition methods. (i) In the first one, the $C^+$ plasma beam of a cathodic arc was quenched in a cold background atmosphere of an inert gas. Mixtures of nitrogen and helium were used. Two series of films were produced, for which the nitrogen/helium ratio was varied in different ways. In the first series (A) the total deposition pressure $P$ was kept constant and the nitrogen partial pressure $P_N$ was varied. In the second series (B), $P_N$ was kept constant and $P$ was varied by varying the amount of helium. (ii) The second deposition technique used a supersonic cluster beam to deposit cluster-assembled carbon.[19]

$sp^2$ phase parameters were obtained by combining different methods. The $sp^2/sp^3$ fraction was determined from carbon *K*-edge EELS.[22] The type of bonding of the $sp^2$ phase was determined using visible (514.5 nm) Raman spectroscopy. A *D* peak in the Raman spectra of amorphous carbons indicates clustering of the $sp^2$ phase into rings.[23] We correlate its increase in intensity relative to the *G* peak, *ID/IG*, to the development of $sp^2$ clusters containing a higher number of rings.[22] The *G* peak arises from all $sp^2$ sites since it is due to the stretching of $sp^2$ C–C bonds. In this work the spectra were fitted with a Breit–Wigner–Fano (BWF) line shape for the *G* peak and a Lorentzian for the *D* peak. The *G* peak position is given as the maximum of the BWF rather than its center to allow a comparison with literature data using a symmetric line shape fitting.[23]

Information about the spatial distribution and correlation of the $sp^2$ clusters was obtained here by comparing the in-plane and transverse resistivities: $\rho_{\parallel}$ and $\rho_{\perp}$. Different values of the two resistivities would indicate an anisotropic development of the $sp^2$ phase (see Sec. IV), as in graphite. $\rho_{\parallel}$ was measured from gap cells defined by lithography on samples deposited on quartz. $\rho_{\perp}$ was obtained by pressing a Pt–Ir tip directly onto films deposited on very highly doped $(n^{++})$Si. In this last case the reproducibility of contact formation was checked, and a contact area of approximately 10 $\mu m^2$ was determined using an optical microscope. We considered a contact area in this range in order to avoid problems related to pin holes. The current–voltage characteristics obtained were symmetric (no rectifying contacts were formed), ohmic at low fields, and showed a field effect at high fields. Resistivity was determined from the low field part of the current–voltage characteristics. For low resistivity samples the data were corrected with a factor taking into account that the tip fringe field lines spread more than the contact area. The anisotropy in bonding can also be detected by EELS.[24]

The surface work function $\phi$ was measured using a Kelvin probe in order to correlate it with changes in the $sp^2$ phase. The probe was a cylinder of 3 mm diameter so that the information obtained is an average, nonlocal one. The local barrier for field emission cannot thus be obtained, however the Kelvin probe measurements give information about the increase in size of the $sp^2$ phase.

Field emission was measured using the parallel plate configuration in a vacuum of about $10^{-8}$ mbar, and spacers located outside the emission region to avoid artefacts due to surface leakage currents. The anode was a patterned indium–tin–oxide plate, coated with a low voltage phosphor. This allowed light emission from an average current density as low as $10^{-9}$ A/cm$^2$ to be recorded. It is acknowledged that the parallel plate method, in contrast to the scanning micrometer sized probe, probes only the most emissive spots. Sometimes, the emission originates from extrinsic effects, such as macroparticle inclusions, or activated damage.[17] However, in general for the emitters investigated here, samples with a lower threshold field also have a higher site density. Hence, although some of the samples studied here are poor emitters, we can still reach some general conclusions on the general factors which effect emission in disordered carbon systems.

## III. RESULTS

### A. Amorphous carbons nanostructured by annealing

There are two effects which characterize the evolution of the $sp^2$ phase with annealing. One is the gradual increase of the $sp^2$ cluster size inside the $sp^3$ matrix. This can be monitored by Raman spectroscopy. The second effect is that the clusters can adopt a preferred direction. This has been shown for deposition at high temperatures, where it was found that the $sp^2$ clusters orient in planes perpendicular to the substrate.[25] Since in systems with mixed $sp^3/sp^2$ phases conduction occurs exclusively in the $sp^2$ phase, anisotropy in conduction can demonstrate the existence of preferred orientations. Here we use Raman spectroscopy and conductivity to investigate how postdeposition annealing affects the $sp^2$ phase in ta-C:N, ta-C:H, and *a*-C:H.

Figure 1 shows, as an example, the evolution of the Raman spectra of ta-C:H with annealing temperature. A clear *D* peak appears at temperatures as low as 400 °C and then continuously evolves at higher temperatures. Gradual $sp^2$ clus-

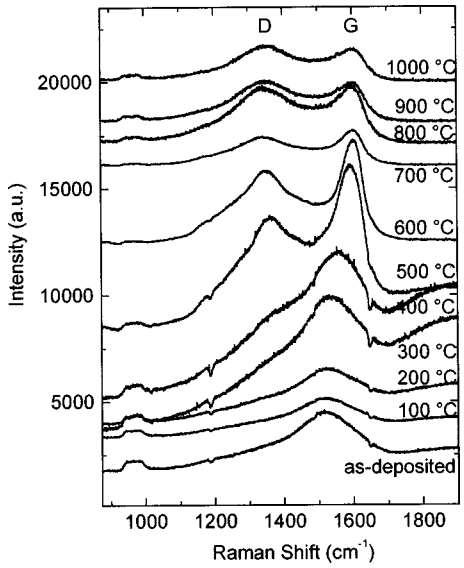


FIG. 1. Evolution of the Raman spectra of ta-C:H with annealing. ta-C:H evolves from amorphous, in the as-deposited state, to nanocrystalline graphite, at the highest annealing temperature.

tering occurs in all the systems (Fig. 2). This is shown by the monotonic increase of $I(D)/I(G)$ with the annealing temperature as $sp^2$ aromatic clusters form in the $sp^3$ matrix. Clustering continues with annealing until the $sp^3$ matrix disappears completely, and then $I(D)/I(G)$ saturates for both *a*-C:H and ta-C:H. For ta-C:N $I(D)/I(G)$ values are lower, indicating that even at high annealing temperatures only small aromatic $sp^2$ clusters are formed. It is important to note that $I(D)/I(G)$ is zero for as-deposited ta-C:N. This means that in this case the as deposited $sp^2$ phase is present only as olefinic, chain-like clusters. Existence of short chains with strong C–C bonds has been predicted in ta-C by theory[26] and is shown in ta-C:N by the high position (at about 1565 $cm^{-1}$ at room temperature) of the *G* peak. At higher annealing temperatures the type of bonding in ta-C:N changes from chains to rings. This contrasts with the situation in *a*-C:H and ta-C:H, where nonzero $I(D)/I(G)$ values

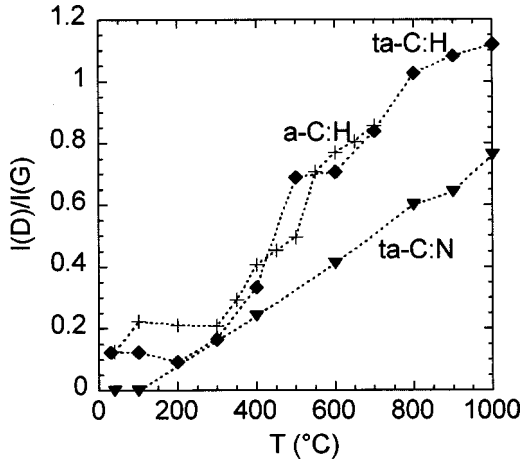


FIG. 2. $sp^2$ clustering induced by annealing *a*-C's is indicated by a gradual increase in the Raman parameter $I(D)/I(G)$.

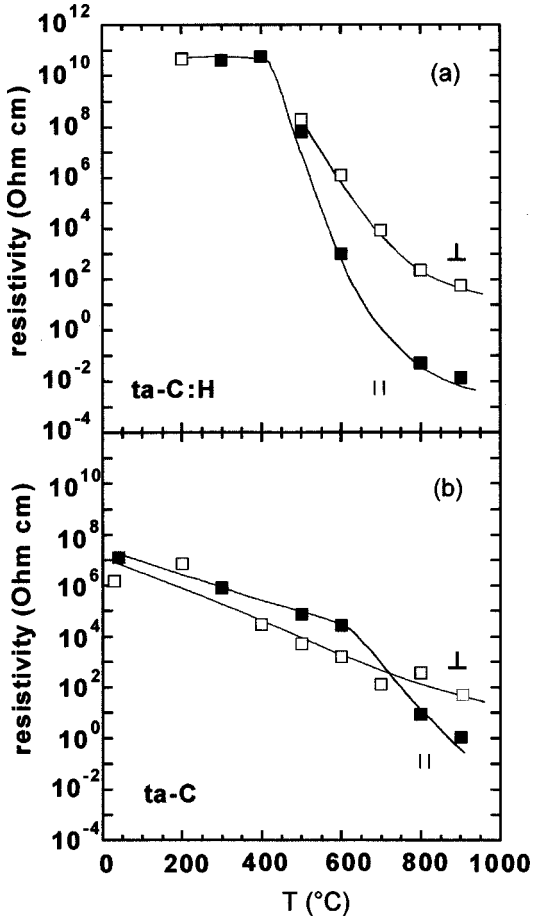


FIG. 3. Resistivity of nanostructured *a*-C's as a function of the anneal temperature. Resistivity was measured in two directions, parallel (∥) and perpendicular (⊥), to the film's substrate for: (a) ta-C:H, and (b) ta-C.

and lower *G* peak positions (~1520 $cm^{-1}$) in the as-deposited state indicate that aromatic rings are present from the beginning.

Resistivity is a more complex property since it depends both on the quantity and quality of the $sp^2$ phase. This is discussed in more detail in Sec. IV. Both $\rho_{\parallel}$ and $\rho_{\perp}$ were measured in order to check if a preferential orientation of the $sp^2$ phase also occurs after postdeposition annealing. Figure 3(a) shows that $\rho_{\parallel}$ and $\rho_{\perp}$ in ta-C:H decrease continuously with annealing. The decrease does not follow a single law, suggesting that there are several stages in the structural transformation induced by annealing. $\rho_{\parallel}$ varies more than $\rho_{\perp}$, so that at 1000 °C $\rho_{\parallel}$ is about $10^{-3}\,\Omega$ cm, 4 orders of magnitude lower than $\rho_{\perp} \approx 10\,\Omega$ cm. These values correspond to conversion into nanocrystalline graphite, which is also indicated by the saturation of $I(D)/I(G)$ (Fig. 2). For comparison, note that for highly oriented pyrolitic graphite the resistivities in the basal plane and along the **c** axis are $\rho_a \approx 10^{-4}\,\Omega$ cm and $\rho_c \approx 10^{-1}\,\Omega$ cm, respectively.[27] These very different values are due to bonding anisotropy in graphite.

To demonstrate that the development of anisotropy in conduction with annealing is not specific to ta-C:H, we also measured the two resistivities in ta-C [Fig. 3(b)]. We again obtained that $\rho_{\parallel}$ varies more than $\rho_{\perp}$. The ta-C used here has

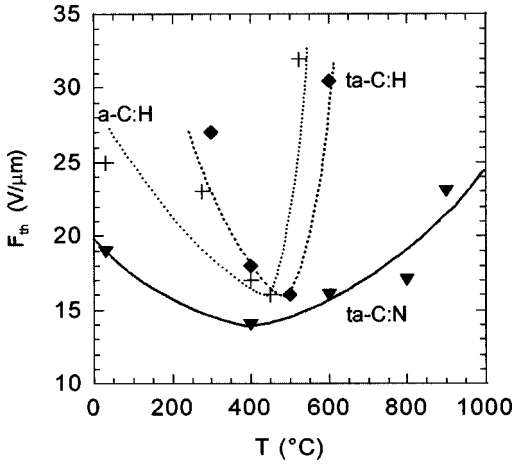


FIG. 4. Emission threshold field in nanostructured *a*-C's with the anneal temperature.

an as-grown $sp^2$ rich surface layer several nm thick, along with buried layers of lower density.[28] These would make it liable to more rapid graphitization than ta-C:H, which possesses a much thinner (less than 1 nm) $sp^2$ rich surface layer.[27] However, the variations in ta-C are less than in ta-C:H, indicating that the more rapid increase of $\rho_{\parallel}$ relative to $\rho_{\perp}$ in both materials is not due to surface graphitization, but related to intrinsic properties of the films. Moreover, the variations in resistivity in ta-C:H are closely related to hydrogen evolution from these films (see Sec. IV). Thus, the different $\rho_{\parallel}$ and $\rho_{\perp}$ values for our films suggest an anisotropic development of the $sp^2$ phase induced by annealing, with the $sp^2$ clusters aligning *parallel* to the substrate. This conclusion is further supported by *K*-edge EELS measurements.[24]

Figure 4 shows the effect of annealing on the field emission threshold $F_{\mathrm{th}}$. In all the systems, $F_{\mathrm{th}}$ first decreases, passes through a minimum, and then increases again. This happens against the continuous decrease in resistivity (Fig. 3). As discussed in Ref. 18, we found no correlation between improvement in emission and changes in the $sp^3$ content. The chemical composition is not a key factor either since an optimum bonding configuration is achieved in all the systems, irrespective of the presence or absence of H or N. Chemical composition only influences $F_{\mathrm{th}}$ indirectly because it affects the $sp^2$ cluster evolution and conductivity (see Sec. IV). Most H evolution from *a*-C:H and ta-C:H is above 500 and 600 °C,[29] respectively, while N is expected not to evolve from this ta-C:N above 700–800 °C.[30]

The surface work function $\phi$ reflects the changes in structure with annealing. In *a*-C:H $\phi$ increases from 3.8–4 eV as deposited to ~4.9 eV after annealing, reflecting the hydrogen loss. As $sp^2$ clustering decreases the optical gap,[31,23] the electron affinity $\chi$ also increases with postdeposition annealing. Thus, the decrease of $F_{\mathrm{th}}$ occurs against an increase in $\phi$ and $\chi$, showing that $\phi$ and $\chi$ are not key parameters for emission. This confirms our previous results on emission from surface treated ta-C.[13]

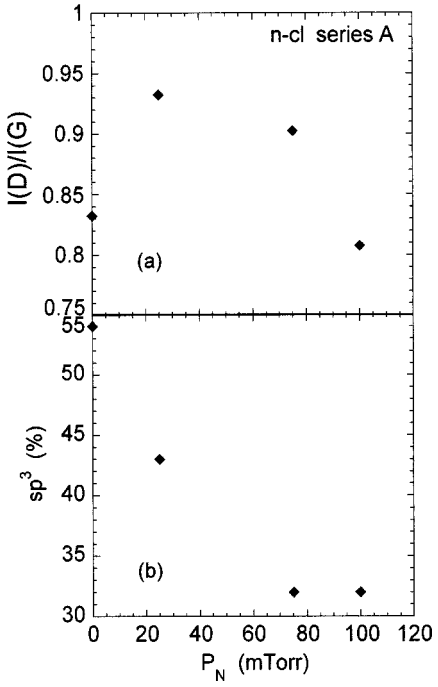


FIG. 5. (a) $I(D)/I(G)$ and (b) $sp^3$ content for *n*-cl carbon films deposited by cathodic arc, using deposition conditions A (constant total pressure and variable nitrogen partial pressure).

### B. As-deposited nanoclustered carbons

We first present results for the films produced in the cathodic arc by quenching a $C^+$ plasma in an inert background atmosphere. Figures 5 and 6 show the $sp^3$ content and $I(D)/I(G)$ for the two series (A and B, respectively) described in Sec. II. For both of them, large $I(D)/I(G)$ val-

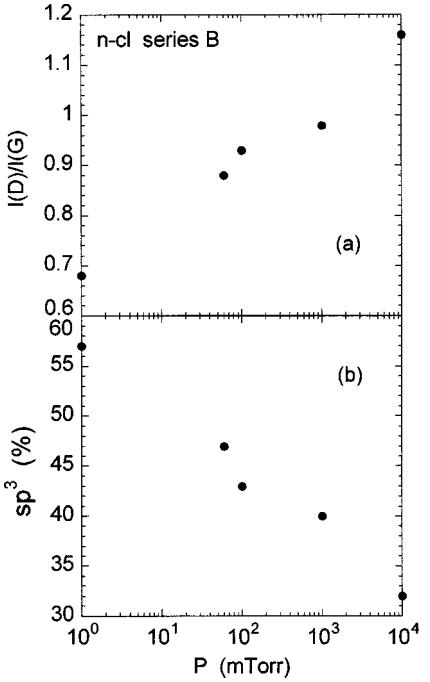


FIG. 6. (a) $I(D)/I(G)$ and (b) $sp^3$ content for *n*-cl carbon films deposited by cathodic arc, using deposition conditions *B* (constant nitrogen partial pressure and variable helium partial pressure).

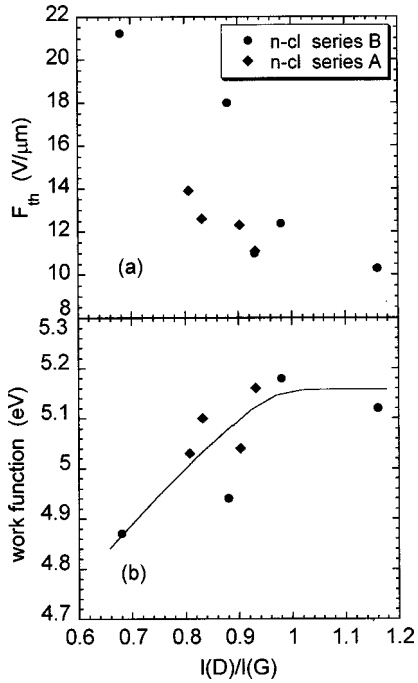


FIG. 7. (a) Emission threshold field and (b) average work function for *n*-cl carbon films deposited by cathodic arc as a function of $I(D)/I(G)$.

ues are obtained [Figs. 5(a) and 6(a)], indicating a high degree of clustering, similar to that of *a*-C:H or ta-C:H films annealed at high temperatures. For series A, $I(D)/I(G)$ reaches a small maximum for $P_N \approx 20$ mTorr, while continuously increasing with the total deposition pressure $P$ for series B. In contrast, the $sp^3$ fraction decreases continuously for both series [Figs. 5(b) and 6(b)]. Even for the highest deposition pressures the films are not completely graphitic, retaining an $sp^3$ content of about 30%.

$F_{\text{th}}$ is found to decrease continuously with increasing clustering [Fig. 7(a)], in contrast to nanostructured *a*-Cs (see Sec. III A), where an optimum bonding was found. This variation is against that of the average work function $\phi$ [Fig. 7(b)]. $\phi$ was found to increase by about 0.4 eV with $I(D)/I(G)$, and saturates for the most clustered films. This shows that $\phi$ can be quite sensitive to the development of larger $sp^2$ domains. In contrast, in nitrogenated ta-C with a N content of less than 10%, where the $sp^2$ clusters remain small and mainly chain-like,[32] $\phi$ remains constant with increasing nitrogen content.[13]

The clustered assembled (ca-C) films can have a 3D structure, with cage-like clusters embedded in an amorphous matrix.[20] These can be as big as 2–3 nm, conferring porosity to the network. Compared to the other nanoclustered films, the ca-C films are well clustered ($I(D)/I(G) \sim 0.7-1$) and have an $sp^2$ content of about 70%–80%. These films show lower threshold field and higher site density than the *a*-C's nanoclustered by postdeposition annealing (see Sec. IV).

## IV. DISCUSSION

The results described in the previous section show that emission generally improves with $sp^2$ clustering, but in some cases there are factors that oppose it. This raises several questions about the $sp^2$ phase structure: is there (i) an optimal size of $sp^2$ clusters, (ii) a preferred orientation or mesoscale organization, or (iii) a favorable surface bonding?

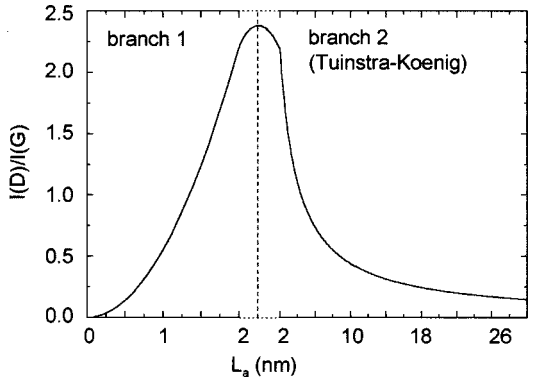


FIG. 8. Generic correlation between $I(D)/I(G)$ and the in-plane correlation length $L_a$ of $sp^2$ aromatic clusters given by Raman spectroscopy.

### A. $sp^2$ cluster size

There is a generic correlation between the in plane correlation length ("size") $L_a$ of $sp^2$ aromatic clusters and $I(D)/I(G)$, as shown in Fig. 8.[33,23] There are two branches corresponding to different degrees of ordering of the $sp^2$ phase. One goes from *a*-C toward nanocrystalline graphite, while the second continues the transition up to polycrystalline and single crystal graphite. The second branch is described by the Tuinstra–Koening (TK) relationship,[34] which states that $I(D)/I(G)$ increases as $1/L_a$ by decreasing the graphitic crystallite size. There is a limit of validity to the TK relationship since for very small $L_a$ the $D$ peak and $I(D)/I(G)$ vanish (Figs. 1 and 2). Branch one shows that for small clusters (as in annealed *a*-C), contrary to the TK relationship, $I(D)/I(G)$ increases with $L_a$ to cross branch two at $L_a \sim 1.5-2$ nm. This corresponds to development and ordering of the $sp^2$ phase inside the $sp^3$ matrix of *a*-C's until nc-C is formed. $I(D)/I(G)$ was then shown to be proportional to the number of aromatic rings in the cluster, and a variation law as $L_a^2$ was proposed.[23] We used this relationship to convert Figs. 4 and 3(a) as a function of $L_a$, into Figs. 9(a) and 9(b), respectively.

Figure 10 shows $F_{\text{th}}$ as a function of $L_a$ for all the films described in Sec. III. All of them correspond to branch one on Fig. 8, as indicated by the width and the position of the Raman *G* peak. We also added a point corresponding to the oriented nanocrystalline graphite material of Obraztsov *et al.*[5] for which an $L_a$ of about 15 nm was determined from the Tuinstra–Koening branch.

It is important to realize that the $L_a$ derived by Raman spectroscopy reflects the extension of *ordered* $sp^2$ domains and not the overall, physical dimension of the $sp^2$ phase, which can be much larger. Due to disorder, micron-sized $sp^2$ particles can have an $L_a$ of 1–2 nm. Another example is ca-C films formed from building blocks which can reach 2–3 nm, yet their $L_a$ can be below 1 nm. Only in cases when small ordered clusters are induced in a disordered matrix, as for annealed *a*-C's, is $L_a$ close to the actual dimension of the $sp^2$ phase. Finally, very small $L_a$s, below 0.3–0.4 nm as deduced

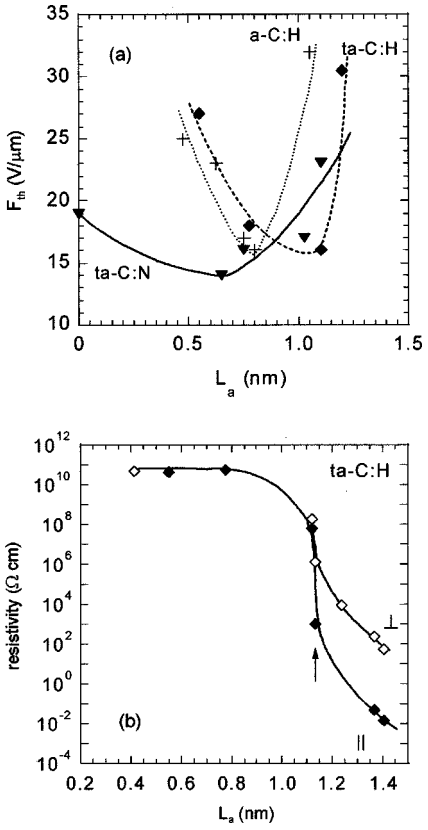


FIG. 9. (a) Emission threshold field and (b) resistivities for nanostructured *a*-C's, as a function of the in-plane correlation length $L_a$ of $sp^2$ aromatic clusters given by Raman spectroscopy. The arrow in (b) indicates the onset of an anisotropic development of the $sp^2$ phase.

from the $L_a^2$ law, are only indicative of very limited $sp^2$ clustering, with a preponderance of chain-like structures.

In these conditions, is $L_a$ given by Raman a good parameter to classify films for electron emission? Figure 10 indicates that this classification is useful if one also includes the $sp^2$ phase orientation and mesoscale organization. Starting from *a*-C's, in which only very small aromatic clusters are present, the emission improves by increasing the size of $sp^2$ clusters distributed randomly in the $sp^3$ matrix. This was attributed to local field enhancement generated by more conductive $sp^2$ clusters embedded in the insulating $sp^3$ matrix.[18] In this case of small clusters, the geometrical dimension of the clusters can be considered as equal to $L_a$. Then, there is a bifurcation point. This point is related to the organization of the $sp^2$ phase at a larger scale, which introduces new properties: the $sp^2$ phase can acquire a preferential 2D orientation, parallel or perpendicular to the substrate, or a more complex 3D topology. As shown in Fig. 10, the development of $sp^2$ clusters in planes perpendicular to the emission direction (as in postdeposition annealed *a*-C's) appears to be unfavorable to emission. However, emission improves when $L_a$ is further increased in films with a more complicated, 3D topology (as for the majority of as-deposited clustered films), to become very good for films with $sp^2$ domains oriented mainly parallel to the emission direction.

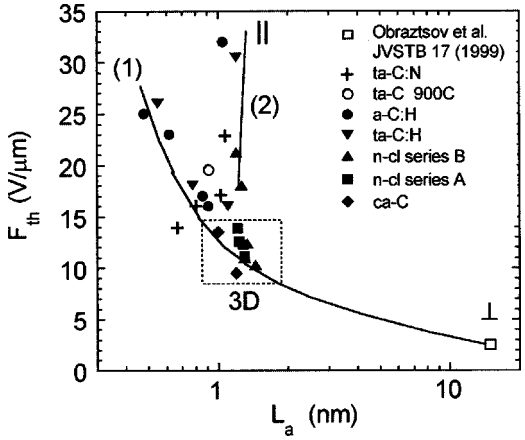


FIG. 10. Emission threshold field as a function of the Raman in-plane correlation length $L_a$ for various classes of carbon films. Going down on curve 1, the emission site density increases.

### B. $sp^2$ phase orientation and topology

In Sec. III it was shown that *a*-C's develop conduction anisotropy with postdeposition annealing. We now formally relate this to the $sp^2$ phase structural anisotropy.

In graphite, the anisotropy in conduction is extreme. There is easy conduction in the basal plane due to delocalization of the $\pi$ electrons over the whole graphitic sheet, while along the **c** axis this is more difficult because of the weak, van der Waals bonding between the graphitic sheets.

In carbons with mixed $sp^2/sp^3$ phases the $sp^2$ sites are generally localized in the $sp^3$ matrix, therefore conduction is described by some kind of hopping between $sp^2$ sites. In *a*-C's, where only small $sp^2$ clusters are present, there is little or no anisotropy in conduction. Transport is described reasonably well, at least over some temperature ranges, by hopping between near-neighbor $sp^2$ sites or clusters[35] [Eq. (1a)], or variable range hopping (VRH) [Eq. (1b)].

$$\rho^{-1}=\frac{K_1 d^2}{T}\exp\left(-\frac{E}{kT}-\frac{2d}{a}\right), \tag{1a}$$

$$\rho^{-1}=\frac{K_2}{[aN(E_f)]^{1/2}}\exp\left\{-\left[\frac{K_3}{a^3 N(E_f)T}\right]^{1/4}\right\}. \tag{1b}$$

$\rho$ depends on the density of states $N(E)$ in which the transport occurs (near the Fermi level if VRH, or at the energy $E$ if near-neighbor hopping), the localization radius $a$ of these states, and the distance $d$ between hopping sites. $K_1$, $K_2$, and $K_3$ are constants. $\rho$ decreases at higher $N(E)$, and with increasing $a$ and decreasing $d$ because this increases the degree of overlap between the electron wave functions of the hopping sites.

Nanostructuring *a*-C's by annealing increases $L_a$ of $sp^2$ clusters, and this should increase $a$ because the $\pi$ electrons in an aromatic ring are delocalized on the whole ring.[30] A complication arises from the fact that the $sp^2$ clusters are embedded in the $sp^3$ diamond-like matrix, so $a$ depends also on the

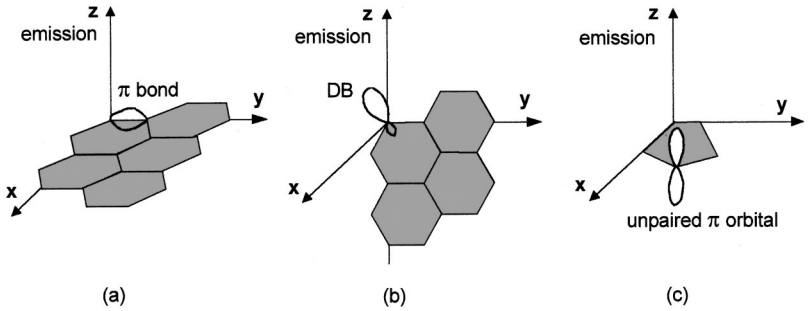


FIG. 11. Surface bonding and orbital orientation relative to the electric field which can occur in carbon films.

position of the $\pi$ band relative to the $\sigma$ band, $E_\pi - E_\sigma$. $E_\pi - E_\sigma$ increases with increasing $L_a$ since the $\pi-\pi^*$ gap decreases.[31] One thus has

$$a = C_1 \frac{L_a}{[E_\pi(L_a) - E_\sigma]^{1/2}}. \tag{2}$$

Moreover, in hydrogenated systems $E_\sigma$ is affected by hydrogen since this bonds preferentially to the $sp^3$ sites. Thus, with hydrogen evolution due to annealing, $E_\sigma$ shifts closer to $E_\pi$. However, for larger $sp^2$ clusters, and after hydrogen evolution from *a*-C:H, the energy dependent factor from Eq. (2) becomes constant and one can approximate

$$a = C_2 L_a. \tag{3}$$

We can now relate the changes in resistivity to $sp^2$ phase clustering in *a*-C's annealed postdeposition. Consequently, $\rho_\parallel$ lower than $\rho_\perp$ implies an anisotropic orientation of the $sp^2$ clusters in planes parallel to the substrate. Note that, in this case, relation (3) applies correctly only to $\rho_\parallel$ and not to $\rho_\perp$. A more quantitative correlation can be found in Ref. 36.

Figures 3(a) and 9(b) show that $\rho_\parallel$ decreases more abruptly in ta-C:H for annealing temperatures above 500 °C. This indicates a sudden development of the $sp^2$ phase in clusters parallel to the substrate (perpendicular to the emission direction), which is related to the onset of hydrogen evolution from these films. H evolution decreases the $\sigma-\sigma^*$ gap, as explained above, and favors an increase in cluster size through $sp^3$ to $sp^2$ conversion (see Figs. 1 and 2). Both effects increase *a*, rapidly decreasing $\rho_\parallel$ [Fig. 9(b)].

As shown in Figs. 9(a) and (b), $F_{\text{th}}$ in ta-C:H reaches its minimum just before the onset of the $sp^2$ phase anisotropy, and then degrades rapidly. There are several reasons for which orientation of the $sp^2$ phase in planes perpendicular to the emission direction can be unfavorable. (i) This spatial configuration decreases the aspect ratio of the $sp^2$ regions embedded in the $sp^3$ matrix, and thus the field enhancement factor. (ii) Field screening can occur when the $sp^2$ islands are too dense or too large. (iii) Large $sp^2$ islands parallel to the substrate behave as equipotentials; they can trap electrons and become negatively charged, repelling the incoming emission electrons back toward the substrate. This can also explain why introduction of $sp^2$ internal layering in ta-C degrades the emission.[37,28]

$sp^2$ clusters aligned on the emission direction should be a more favorable configuration because they provide: (i) better transport, (ii) a better field enhancement factor, and, in some cases, (iii) a more favorable electronic configuration at the surface (see Sec. IV C). Note, however, that in order to take advantage of this configuration the clusters should not be dispersed too densely to avoid screening effects.

The as-deposited nanoclustered films described in Sec. III B are better emitters, with lower threshold fields and higher site density, lying on curve 1 in Fig. 10. Their common characteristic is that all have a more 3D structure. The ca-C films consist of a distribution of smaller and bigger clusters, some of them fullerenes.[21] The majority of the films deposited in the cathodic arc consist of smaller, nonfullerene type clusters, but with a 3D mesoscale topology. This was shown by high resolution scanning electron microscopy and, indirectly, by their porosity. Several nanoclustered films obtained in the cathodic arc lie on curve 2 in Fig. 10, and are more similar to the *a*-C's annealed at high temperatures, being compact, without porosity.

There are several reasons for which good emission can occur from 3D nanoclustered carbon films. The 3D topology can accommodate higher $sp^2$ cluster sizes oriented on the emission direction, without inducing a field screening effect, while the presence of both $sp^2/sp^3$ phases guarantees a way to obtain local field enhancement. Finally, as discussed below, a defective 3D structure can provide highly localized states oriented on the emission direction through which emission is facilitated.

### C. Surface electronic structure

The electronic bonding at the film's surface is also of importance. Considering the extreme case of nanotubes (NTs), these are good electron emitters mainly because of their high aspect ratio which generates very high local field, and because of their high conductivity along the emission direction. However, it has been found that emission from NTs is controlled not only by the geometric field enhancement factor but also depends on the tube end configuration.[38–40]

The type of surface bonding can induce localized states deep in the gap. Localized states near or above the Fermi level can facilitate emission. These states exist[41,15] and appear to help emission from NTs. The directionality of the bonds is also important since the tunneling effect which governs the electron emission is highly anisotropic. Thus, an electron orbital aligned parallel to the electric field will give a higher tunneling probability.

Figure 11 shows several situations. Figure 11(a) shows a graphene sheet with the basal plane perpendicular to the

emission direction. In this case, on the emission direction there are only $\pi$ bonds which do not give states in the band gap. This unfavorable situation occurs for the *a*-C's annealed postdeposition at high temperatures (curve 2 on Fig. 10). Figure 11(b) shows the opposite situation of the graphene sheet oriented on the emission direction. Dangling bonds occur at the vacuum end because of the breaking of the $\sigma$ bonds of the $sp^2$ orbitals, which create localized states in the band gap with a maximum electronic density on the field direction. This seems to be a very favorable situation. However, such dangling bonds are very reactive and tend to be passivated by chemisorbed hydrogen. Therefore, C dangling bonds are possible only in high vacuum, or by breaking of C–H bonds under conditions of very high local field or high temperature caused by intense emission current. Figure 11(c) shows a pentagon, which is the configuration which introduces a convex curvature in nitrogen rich *a*-C,[42] 3D nanostructured films, or capped nanotubes. The unpaired $\pi$ orbital gives a localized state in the gap oriented in the field direction, which is also chemically stable. Moreover, an unpaired $\pi$ orbital can also occur in bent vertical graphene sheets, which are claimed by Obraztsov *et al.*[43] to be present in their highly oriented graphitic films. The unpaired $\pi$ orbital thus appears as the most favorable stable electronic configuration for field emission.

Finally, is the idea of correlating emission sites with $sp^2$ clusters of certain properties consistent with the site densities observed experimentally? The films considered here were chosen with the scope of having the cluster size defined by Raman as a continuously varying parameter. Site densities counted using a phosphor screen were also found to vary continuously for the films on curve 1 in Fig. 10. Emission is scarce (from only several sites) and, sometimes, of extrinsic origin for the as-deposited amorphous carbon films, but it increases to about $10^2$sites/cm$^2$ for the annealed *a*-C's; the site density then varies from $10^2$ to more than $10^3$ for the cluster assembled films, and to more than $10^4$sites/cm$^2$ for the nanoclustered films obtained in the cathodic arc.[8] One notes that even the highest of these values are less than what one would expect from a one-to-one correlation with the number of clusters present in a material with a dominant $sp^2$ phase. The site density of our *n*-cl films from cathodic arc could be highly raised without requiring very high fields using the well-known technique of the resistive (ballast) layer.[44] In this way, an almost uniform emission was visualized in films with high cluster sizes and number of clusters. This also shows that factors not discussed here, such as moderate inhomogeneities in roughness (affecting the geometrical field factor at the emission site) or in local conductivity, preclude observation of even emission from all the potential emission sites.

A direct correlation between the presence of $sp^2$ nanostructures and emission sites cannot be made on the basis of these results, as scanning probe techniques sensitive at nanometer scale are required by the size of the $sp^2$ features involved. The results of such a study performed on the nanoclustered cathodic arc and clustered assembled carbon films will be presented elsewhere.[45] A direct identification of subnanometer narrow $sp^2$ regions in a diamond matrix as the emitting sites was, however, obtained in the case of thin ($\sim$100 nm) ultrananocrystalline diamond (UNCD) films.[46] This material consists of 2–5 nm size crystalline diamond grains and is devoid of intergranular amorphous carbon or graphitic phases, as opposed to nanocrystalline diamond with 50–100 nm size grains and a significant intergranular nondiamond phase. In UNCD the only $sp^2$ bonded zones are $<1$ nm wide channels inbetween the grains, which were identified as depressions in topographic STM scans, but as emission sites in local field-emission mappings.[46] Note that the small width of these $sp^2$ regions made the correlation with the emission sites somewhat less ambiguous than in the case of nanocrystalline diamond, where the $sp^2$ rich intergranular regions were much more extended and structurally more nonhomogeneous.

## V. CONCLUSION

We studied field emission from various nanostructured carbons. The effect of different $sp^2$ phase parameters, such as cluster size, orientation and topology, and electronic disorder, are emphasized and discussed. It is found that increasing the cluster size derived from Raman spectroscopy in the 1–10 nm range improves emission. The emission can be limited by the specific topology adopted by the $sp^2$ phase. $sp^2$ phase ordering in graphitic planes perpendicular to the emission direction is found to be clearly unfavorable to emission. Films with a 3D topology are better emitters. This is attributed to a higher degree of $sp^2$ clustering on the emission direction, and to defects creating highly localized states oriented parallel to the applied electric field. $sp^2$ clusters embedded in the $sp^3$ matrix or spatially confined defects inducing strong electronic disorder can provide local field enhancement to facilitate emission.

## ACKNOWLEDGMENTS

The authors thank Professor C. E. Bottani for permission to use the Raman facilities. A. I. gratefully acknowledges a Research Fellowship from Girton College, Cambridge, while A.C.F. acknowledges an E.U. Marie Curie Fellowship. Cluster assembled carbon was produced at the University of Milano under Advanced Research Project CLASS.

[1] A. A. Talin, L. S. Pan, K. F. McCarty, T. E. Felter, H. J. Doerr, and R. F. Bunshah, Appl. Phys. Lett. **69**, 3842 (1996).
[2] A. R. Krauss, D. M. Gruen, D. Zhou, T. G. McCauley, L. C. Qin, T. Corrigan, O. Auciello, and R. P. H. Chang, Mater. Res. Soc. Symp. Proc. **495**, 299 (1998).
[3] O. Groning, O. M. Kuttel, P. Groning, and L. Schlapbach, J. Vac. Sci. Technol. B **17**, 1970 (1999).
[4] A. V. Karabutov, V. G. Ralchenko, S. K. Gordeev, and P. I. Belobrov, Proceedings 18th NATO Summer School: Nanostructured Carbon for Advanced Applications, Erice, 19–31 July, 2000.
[5] A. N. Obratsov, I. Yu. Pavlovsky, and A. P. Volkov, J. Vac. Sci. Technol. B **17**, 674 (1999).
[6] V. I. Merkulov, D. H. Lowndes, and L. R. Baylor, Appl. Phys. Lett. **75**, 1228 (1999).
[7] G. A. J. Amaratunga *et al.*, New Diamond Front. Carbon Technol. **9**, 31 (1999).
[8] B. S. Satyanarayana, J. Robertson, and W. I. Milne, J. Appl. Phys. **87**, 3126 (2000).
[9] B. F. Coll, J. E. Jaskie, J. L. Markham, E. P. Menu, A. A. Talin, and P. von Allmen, Mater. Res. Soc. Symp. Proc. **498**, 185 (1998).
[10] A. C. Ferrari, B. S. Satyanarayana, J. Robertson, W. I. Milne, E. Barborini,

P. Piseri, and P. Milani, Europhys. Lett. **46**, 245 (1999).
[11] J. Robertson, J. Vac. Sci. Technol. B **17**, 659 (1999).
[12] J. Schafer, J. Ristein, and L. Ley, J. Vac. Sci. Technol. A **15**, 408 (1997).
[13] A. Ilie, A. Hart, A. J. Flewitt, J. Robertson, and W. I. Milne, J. Appl. Phys. **86**, 6002 (2000).
[14] O. Groening, O. Kuettel, P. Groening, and L. Schlapbach, Appl. Phys. Lett. **71**, 2253 (1997).
[15] K. A. Dean, O. Groening, O. M. Kuttel, and L. Schlapbach, Appl. Phys. Lett. **75**, 2773 (1999).
[16] J. Robertson, Mater. Res. Soc. Symp. Proc. and references therein (in press).
[17] O. Groning, O. M. Kuttel, P. Groning, and L. Schlapbach, J. Vac. Sci. Technol. B **17**, 1064 (1999).
[18] A. Ilie, A. C. Ferrari, T. Yagi, and J. Robertson, Appl. Phys. Lett. **76**, 2627 (2000).
[19] P. Milani, M. Ferretti, P. Piseri, C. E. Bottani, A. Ferrari, A. Li Bassi, G. Guizzetti, and M. Patrini, J. Appl. Phys. **82**, 5793 (1997).
[20] P. Milani, A. Podesta, P. Piseri, E. Barborini, C. Lenardi, and C. Castelnovo, Diamond Relat. Mater. **10**, 240 (2001).
[21] D. Donadio, L. Colombo, P. Milani, and G. Benendek, Phys. Rev. Lett. **83**, 776 (1999).
[22] P. J. Fallon, V. S. Veerasamy, C. A. Davis, J. Robertson, G. A. J. Amaratunga, W. I. Milne, and J. Koskinen, Phys. Rev. B **48**, 4777 (1993).
[23] A. C. Ferrari and J. Robertson, Phys. Rev. B **61**, 14905 (2000).
[24] J. Yuan, A. C. Ferrari, and V. Stolojan (unpublished work).
[25] J. Kulik, G. Lempert, C. Grossman, and Y. Lifshitz, Mater. Res. Soc. Symp. Proc. **593**, 305 (2000).
[26] T. Kohler, Th. Frauenheim, and G. Jungnickel, Phys. Rev. B **52**, 11837 (1995); N. A. Marks, D. R. McKenzie, B. A. Pailthorpe, M. Bernasconi, and M. Parinello, *ibid.* **54**, 9703 (1996).
[27] M. S. Dresselhaus and G. Dresselhaus, Adv. Phys. **30**, 139 (1981).
[28] A. LiBassi, A. C. Ferrari, B. K. Tanner, V. Stolojan, L. M. Brown, and J. Robertson, Diamond Relat. Mater. **9**, 771 (2000).
[29] J. Ristein, R. T. Stief, L. Ley, and W. Beyer, J. Appl. Phys. **84**, 3836 (1998); N. M. J. Conway, A. C. Ferrari, A. J. Flewitt, J. Robertson, W. I. Milne, A. Tagliaferro, and W. Beyer, Diamond Relat. Mater. **9**, 7651 (2000).
[30] D. G. McCulloch and A. R. Merchant, Thin Solid Films **290–291**, 99 (1996).
[31] J. Robertson and E. P. O'Reilly, Phys. Rev. B **35**, 2496 (1987).
[32] B. Kleinsorge, A. C. Ferrari, J. Robertson, and W. I. Milne, J. Appl. Phys. **88**, 1149 (2000).
[33] J. Robertson, Prog. Solid State Chem. **21**, 199 (1991).
[34] F. Tuinstra and J. L. Koening, J. Chem. Phys. **58**, 1126 (1970).
[35] D. Dasgupta, F. Demichelis, and A. Tagliaferro, Philos. Mag. B **63**, 1255 (1991).
[36] A. Ilie, Diamond Relat. Mater. **10**, 207 (2001).
[37] B. S. Satyanarayana, A. Hart, W. I. Milne, and J. Robertson, Appl. Phys. Lett. **71**, 1430 (1997).
[38] J.-M. Bonard, J.-P. Salvetat, T. Stockli, and W. A. de Heer, Appl. Phys. Lett. **73**, 918 (1998).
[39] W. A. de Heer, A. Chatelain, and D. Ugarte, Science **270**, 1179 (1995).
[40] Y. Saito, K. Hamaguchi, R. Mizushima, S. Uemura, T. Nagasako, J. Yotani, and T. Shimojo, Appl. Surf. Sci. **146**, 305 (1999).
[41] D. L. Carroll, P. Redlich, P. M. Ajayan, J. C. Charlier, X. Blase, A. De Vita, and R. Car, Phys. Rev. Lett. **78**, 2811 (1997).
[42] H. Sjostrom, S. Stafstrom, M. Boman, and J.-E. Sundgren, Phys. Rev. Lett. **75**, 1336 (1995).
[43] A. N. Obratsov, A. P. Volkov, I. Yu. Pavlovskii, A. L. Chuvilin, N. A. Rudina, and V. L. Kuznetsov, JETP Lett. **69**, 411 (1999).
[44] J. B. Cui, J. Robertson, and W. I. Milne, J. Appl. Phys. (in press).
[45] C. Ducati and A. Ilie (unpublished).
[46] A. R. Krauss *et al.*, J. Appl. Phys. **89**, 2958 (2001).